Meteorol. Atmos. Phys. 49, 19–41 (1992)

Meteorology and Atmospheric Physics

551.553.11

Department of Marine, Earth and Atmospheric Sciences, North Carolina State University, Raleigh, U.S.A.

A Three-Dimensional Numerical Sensitivity Study of Mesoscale Circulations Induced by Circular Lakes

Z. Boybeyi and **S. Raman**

With 16 Figures

Received December 19, 1991
Revised April 7, 1992

Summary

A three-dimensional mesoscale planetary boundary layer model with the E-ε turbulence closure is used to simulate airflow over a lake of circular shape. A series of model sensitivity studies are performed to examine the effects of lake-land temperature difference, ambient wind magnitude and direction, lake size, surface roughness, the Coriolis force and baroclinic ambient wind conditions on mesoscale lake circulations.

The lake-land temperature difference is essentially the basic energy source driving the mesoscale circulations over the lake on synoptically undisturbed days. A lake-breeze convergence zone is predicted by the model due to the differential heating between the land and the water. It is found that spatial and temporal variations of this convergence zone and associated convection are strongly controlled by the direction and the magnitude of the ambient wind. Under southeasterly and southwesterly ambient winds, the lake-breeze convergence zone and the associated convection occur primarily along upwind and lateral sides of the lake with reference to the general direction of the ambient flow. In contrast to the southeasterly and southwesterly ambient winds, the lake-breeze convergence zone and the convection are predicted all around the coastline of the lake under calm wind.

The model also predicts a cloudless region over the lake in all the case studies due to divergent nature of the lake-breeze circulation. The lake size is found to have a significant effect in intensifying convection. Surface roughness over the land surface is found to be important in determining the intensity of the convection. The combined effect of the Coriolis force and the differential surface roughness between land and water appear to be the responsible mechanism for producing the asymmetric shape of the lake-breeze convergence zone around the symmetric circular lake. Finally, it was found that an initial baroclinic flow has different mesoscale lake-breeze circulation patterns as compared to an initial barotropic flow.

1. Introduction

Lake-breeze circulations (especially the Great lakes of the United States) have been the subject of several observational and numerical investigations (e.g., Briggs and Graves, 1962; Lavoie, 1972; Walsh, 1974; Neumann and Mahrer, 1975; Estoque, 1981; Estoque and Gross, 1981; Hjelmfelt and Braham, 1983; Hjelmfelt, 1990). Observational studies of lake-breezes (and other similar mesoscale circulations) have demonstrated that poor resolution in weather-observing network systems creates problems in developing routine forecasts of this phenomenon. Numerical studies suggest that a more complete picture requires an examination of the effect of the environment on the lake-breeze circulation in order to obtain a better understanding of mesoscale lake-breeze circulations.

For example, Lovaie (1972) has found that changes in the ambient flow across lake Erie produced changes in the storm pattern and precipitation. The lake-land surface temperature difference was found to be the major driving force in his simulations. Lake and land-breeze circulations over circular lakes for two different lake sizes have been investigated by Neumann and Mahrer (1975).

They found that the small lake is more strongly divergent. A three-dimensional structure of the lake-land breeze circulation induced by lake Ontario has been studied by Estoque and Gross (1981). A series of numerical simulations were made to examine the effects of topography and the ambient flow (calm and southerly) on the lake induced circulation. They found that both the magnitude of ambient wind and the topography can have important influence on the lake induced circulation. Although their numerical simulations have been successful, they concluded that further extension of numerical studies such as the effect of vertical wind shear and time variations of the large-scale ambient flow pattern would be desirable. Recently, a more comprehensive numerical study was made by Hjelmfelt (1990). A series of model studies were performed to examine the effects of lake-land temperature difference, atmospheric boundary layer stability, humidity and wind speed and direction on the pattern of lake effect snowstorms downwind of lake Michigan. Their results confirmed the strong effects of lake-land temperature difference, wind speed and temperature lapse rate on lake induced circulation.

These studies clearly indicate importance of environmental factors on the lake-breeze circulations. The purpose of this study is to investigate the modification of airflow over a circular lake for different environmental conditions. A series of basic sensitivity studies are performed to understand the physical processes associated with the lake-breezes using a three-dimensional mesoscale planetary boundary layer model. The model physics include explicit moisture information. An application of this model to the case of circular lake will not only provide a more complete picture of the effect of the environment on the lake-breeze circulation but also will allow us to investigate the complex interaction between cloud scale and mesoscale air motions. The sensitivity studies include influences of lake-land temperature difference, wind speed and direction, lake size, surface roughness, the Coriolis force and baroclinic ambient wind conditions on mesoscale lake-breeze circulation and associated convection.

2. Model Description and Numerical Experiments

The mesoscale numerical model used in this study is the one described by Huang and Raman (1991) and Huang (1990). The model is hydrostatic and anelastic in a terrain-following coordinate system. The prognostic model equations include the horizontal momentum equations, the thermodynamic equation for the potential temperature, and the conservation equations for water vapor, cloud water and rain water. The atmospheric planetary boundary layer (PBL) is treated in two parts as the surface layer and the transition layer. The similarity stability functions given by Businger et al. (1971) are used to account for the surface layer turbulent transport. Above the surface layer, a turbulence closure scheme based on prognostic equation of the turbulent kinetic energy (TKE) and dissipation (ε) is incorporated with the level 2.5 scheme of Mellor and Yamada (1982) to determine eddy diffusivities in the transition layer.

To account for advection effects, a modified version of Warming–Kutler–Lomax advection scheme (Warming et al., 1973) is used in the horizontal and the quadratic upstream interpolation in the vertical. The radiation scheme incorporates the longwave and shortwave radiative transfer. It is essentially similar to the one used by Mahrer and Pielke (1977). This scheme takes into account the absorption of shortwave radiation by water vapor and the longwave energy emitted by water vapor and carbon dioxide. The mesoscale model is initialized based on a 1-D PBL model solving the Ekman-gradient wind equations (for more information see Huang and Raman, 1988). At the lower boundary, a no-slip condition is imposed for the wind. The sea surface temperature is fixed and the ground temperature is computed using the surface energy budget equation in which the longwave and shortwave radiation, the soil heat flux and the turbulent mixing of sensible and latent heat fluxes are used to calculate the equilibrium surface temperatures. For the land surface, relative humidity remains unchanged, but the air in contact with the water surface is assumed to be saturated. At the upper boundary, a radiation boundary condition (Klemp and Durran, 1983) is used to determine the upper perturbation pressure. For the prognostic variables, Orlanski's radiation condition (Orlanski, 1976) with forward-upstream scheme (Miller and Thorpe, 1981) is applied to the lateral inflow boundary grids, while the prediction equations are used at the lateral outflow boundary grids.

Seven numerical sensitivity studies are performed

to investigate the effects of different environmental parameters on mesoscale lake-breeze circulations. In the numerical simulations two different ambient wind directions are considered: southeasterly and southwesterly. Case C1 is designed to investigate the influence of southeasterly ambient wind direction on the lake-breezes, while Case C2 is for the influence of southwesterly ambient wind direction. The selected wind speed ($6\,m\,s^{-1}$) and lake size (60 km radius) are kept identical in these two case studies for direct comparison of the results. Case C3 examines the influence of the lake size by reducing the lake radius to 44 km. All the other prescribed parameters in the model for Case C3 are kept the same as those in Case C2. The influence of ambient wind speed is examined in Case C4 by assuming calm southwesterly winds. Since the differential surface roughness between land and water is one of the important factors in causing mesoscale convergence, it was decided to investigate the relative importance of the differential surface roughness on lake-breeze circulation in Case C5. Case C6 is designed to investigate the influence of the Coriolis force on mesoscale lake-breeze circulation. Finally, Case C7 is designed to examine the influence of baroclinic ambient wind conditions on the lake-breeze circulations. A complete description of all the cases is given in Table 1.

Barotropic ambient wind conditions are assumed initially for all the simulations except for Case C7, with a constant vertical potential temperature gradient of 4 C/km and 80% relative humidity below 2 km. The relative humidity is then assumed to decrease linearly to zero at 5 km height. The value of Coriolis parameter used in the model is for 25 latitude. The model domain contains 20 levels in the vertical with the model top at 7 km. The horizontal domain includes a matrix of 51×51 points with a uniform grid interval of 8 km. The model is integrated for 14 hours for the consideration of the lake-breeze heating cycle with an integration time interval of 30 s. The initial surface temperatures over both the land and the water were set to be 25 C with the variation of soil temperatures determined by diurnal heating. The surface roughness is assumed to be 4 cm over land, while Charnock's relationship is used over the water.

3. Discussion of Results

3.1 Case C1. Southeasterly Wind

In order to examine the influence of ambient wind direction on lake-breeze patterns and associated convection a southeasterly flow of about $6.0\,m\,s^{-1}$ ($U_g = -4.2\,m\,s^{-1}$ and $V_g = 4.2\,m\,s^{-1}$) is used over a circular lake with a radius of 60 km in this case study.

The low-level horizontal pressure field (P), potential temperature field (θ) and horizontal winds (U and V) at 50 m after 3, 6, 9 and 12 hours of simulation are shown in Figs. 1, 2 and 3, respectively.

Table 1. *Description of the Numerical Experiments*

Cases	Geostrophic wind ($m\,s^{-1}$)	Direction	Remarks
C1. The influence of southeasterly wind	$U_g = -4.2$ $V_g = 4.2$	135°	The lake radius is 60 km
C2. The influence of southwesterly wind	$U_g = 4.2$ $V_g = 4.2$	225°	The lake radius is 60 km
C3. The influence of the lake size	$U_g = 4.2$ $V_g = 4.2$	225°	The lake radius is 44 km
C4. The influence of calm wind	$U_g = 0.1$ $V_g = 0.1$	225°	The lake radius is 60 km
C5. The influence of surface roughness	$U_g = 4.2$ $V_g = 4.2$	225°	The lake radius is 60 km
C6. The influence of the Coriolis force	$U_g = -4.2$ $V_g = 4.2$	135°	The lake radius is 60 km The Coriolis force is ignored
C7. The influence of baroclinity	$U_g = -4.2$ $V_g = 4.2$	135°	The lake radius is 60 km

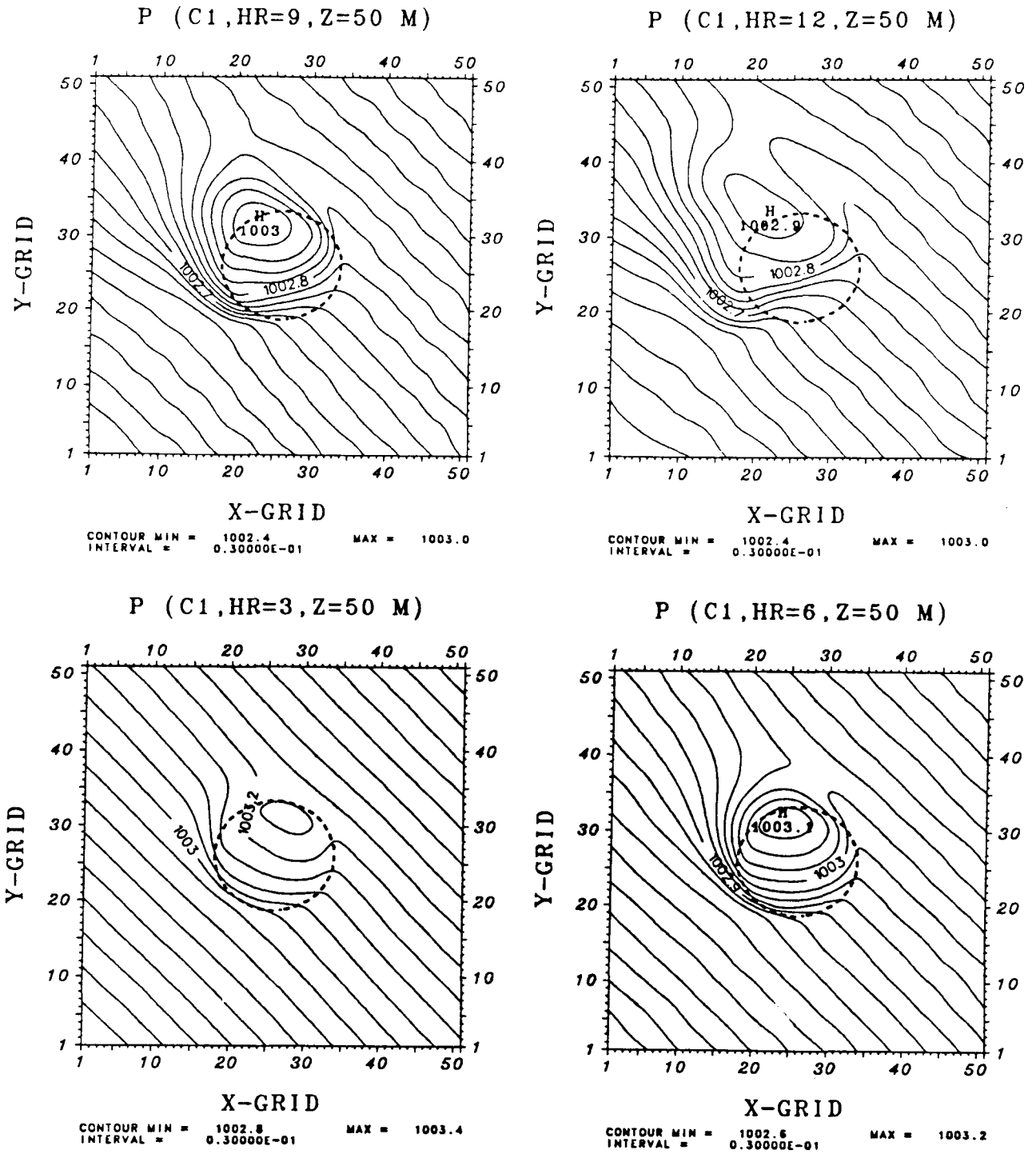

Fig. 1. The low-level pressure field P (mb) at 50 m after 3, 6, 9 and 12 hours of simulation for the southeasterly wind Case C1. The extreme is indicated by letter H (High)

The lake-land temperature difference is essentially the basic energy source driving meso-scale circulations on synoptically undisturbed days. The continuous differential heating between land and water results in vertical thermal mixing in the planetary boundary layer. This creates a lower pressure region at the surface over land causing the winds to turn towards this region. For example, during the early morning hours the pressure surfaces become uniform (not shown). By the third hour after

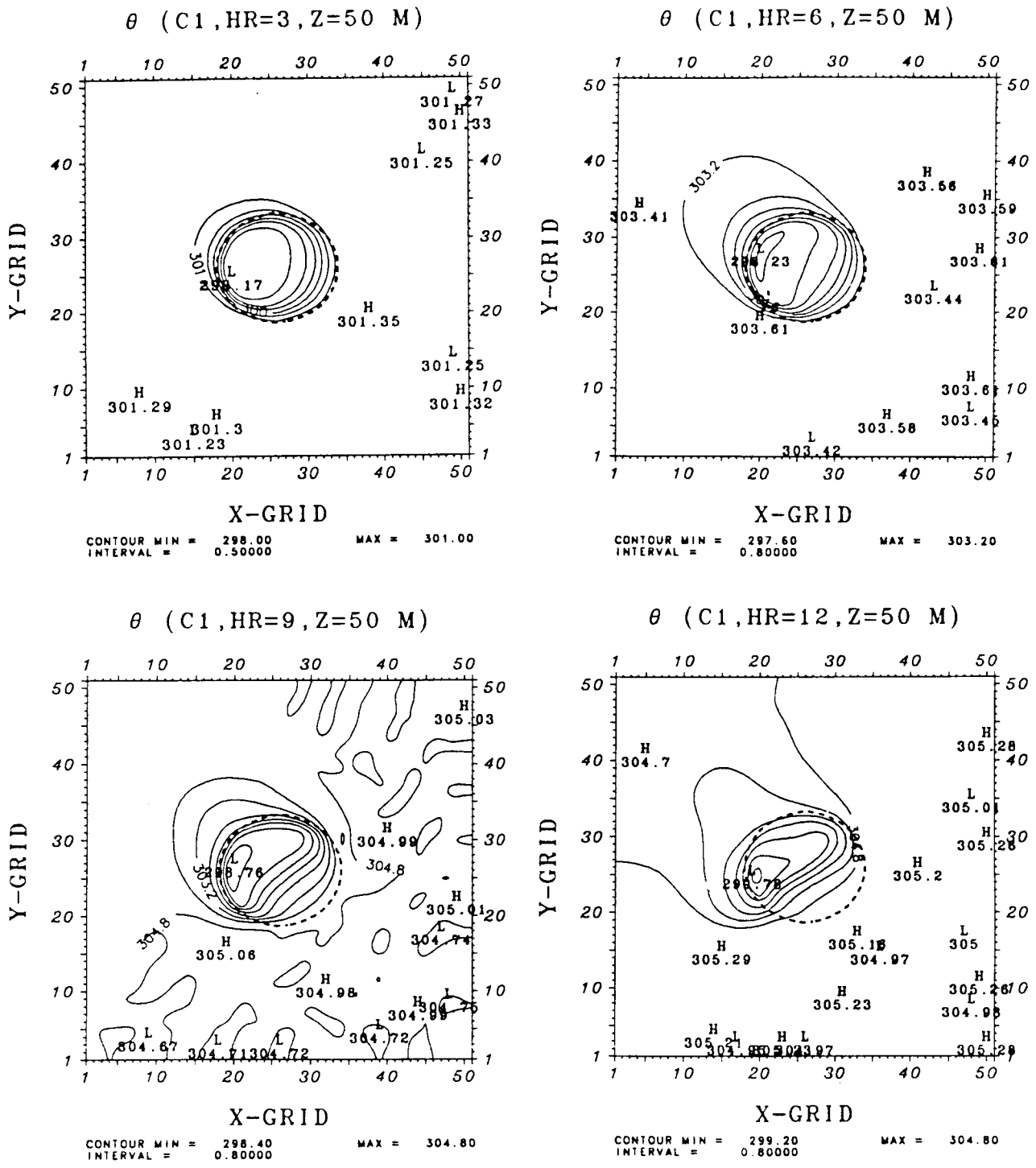

Fig. 2. The low-level potential temperature field θ (°K) at 50 m after 3, 6, 9 and 12 hours of simulation for the southeasterly wind Case C1. The extremes are indicated by letters *H* (High) and *L* (Low)

sunrise, a horizontal pressure gradient (Fig. 1a) and horizontal potential temperature gradient (Fig. 2a) begin to form as a result of continuous differential heating between the land and the water. Hence, the corresponding predicted low-level winds (Fig. 3a) become easterly over the lake in response to the large pressure fall over land on the west side of the lake.

By the sixth hour, a high pressure region along the downwind (northwest) side of the lake and a

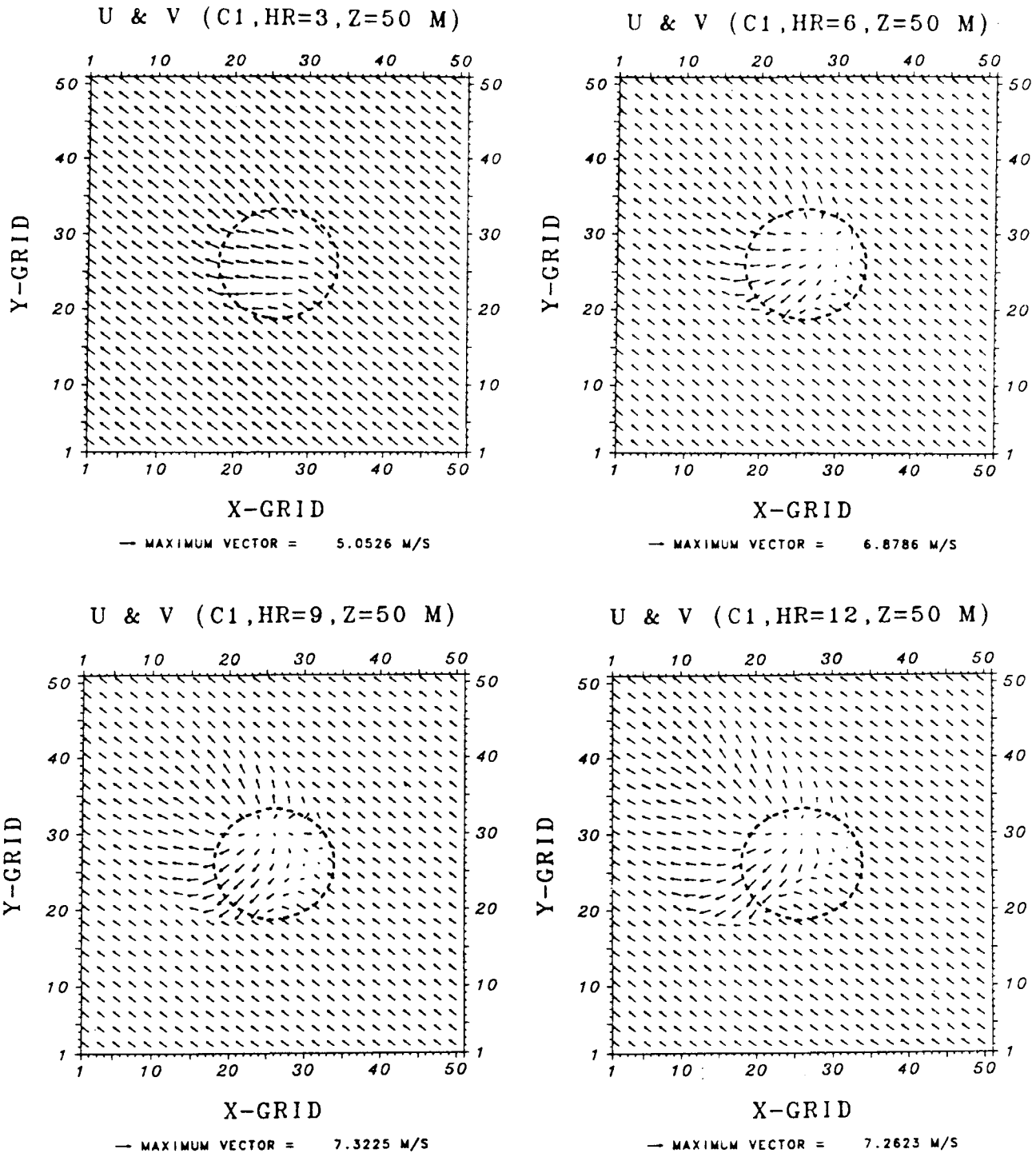

Fig. 3. The low-level horizontal winds U and V ($m\,s^{-1}$) at 50 m after 3, 6, 9 and 12 hours of simulation for the southeasterly wind Case C1

strong pressure gradient along the upwind (southeast) and the lateral (southwest and northeast) sides of the lake are obvious in Fig. 1b. By this time, the southeasterly ambient winds advect warmer land air over relatively cooler lake along the upwind side of the lake creating a well defined horizontal temperature gradient. In contrast, cooler lake air is advected over relatively warmer land along the downwind side of the lake diminishing the horizontal temperature gradient (Fig. 2b).

Subsequently, low-level horizontal winds (Fig. 3b) turn inland in all directions almost normal to the coastlines over the lake in response to the pressure fall over the land thus opposing the southeasterly ambient wind along the upwind and the lateral sides of the lake. This results in a well defined divergence region over the lake and a lake-breeze convergence zone along the upwind and the lateral sides of the lake. The convergence zone doesn't form along the downwind side of the lake due to

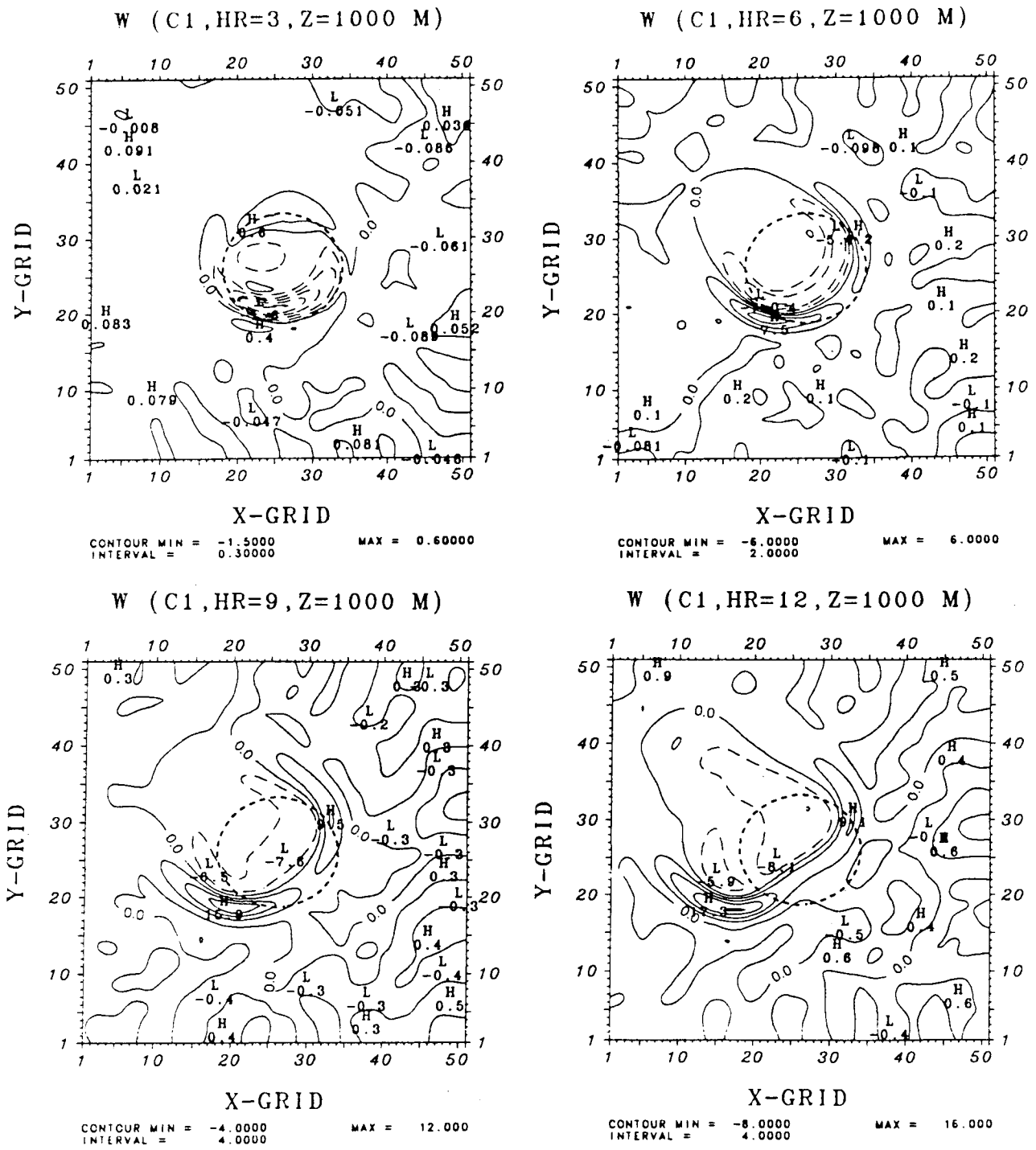

Fig. 4. The vertical velocity W (cm s^{-1}) at 1000 m after 3, 6, 9 and 12 hours of simulation for the southeasterly wind Case C1. The extremes are indicated by letters H (High) and L (Low)

the local lake-breeze being in the same direction as the ambient flow. The winds increase in speed due to the acceleration of the air towards the region of lower pressure by this hour. The size of the arrows is proportional to the wind speed. The strongest horizontal winds form over the southwest lateral side of the lake due to the large horizontal pressure gradients and potential temperature gradients over this area.

By the ninth and twelfth hours, strong on-shore winds of the lake-breeze along the southwest lateral side of the lake advect relatively cooler lake air over the land resulting in the advection of both the horizontal pressure gradients (Figs. 1c, d) and the potential temperature gradients (Figs. 2c, d). This causes the lake-breeze convergence zone (Figs. 3c, d) to advect further inland along this region, while the convergence zone remains essentially stationary along the other lateral side (northeast) of the lake. The inland penetration of the lake-breeze convergence zone mainly depends on the intensity of the total heat input to the atmosphere (e.g., see Pearson, 1973). The horizontal pressure gradients and potential temperature gradients along the upwind and the downwind sides of the lake and hence the lake-breeze convergence zone along the upwind side of the lake are also advected by the southeasterly ambient winds. These processes cause the lake-breeze convergence zone to have an asymmetric shape in the later afternoon. This asymmetric shape could be due to two factors: 1) the differential surface roughness between the land and the water and 2) the Coriolis force. The influence of the differential surface roughness and the Coriolis force will be examined in detail separately in Case C5 and Case C6, respectively.

The predicted vertical velocities (W) at 1000 m after 3, 6, 9 and 12 hours of simulation for the southeasterly ambient wind case are shown in Fig. 4. The results are presented at the average height where largest vertical velocities occur. In Fig. 4, upward motions are represented by solid contours, while downward motions are represented by long dashed contours and their extremes by letters, H (High) or L (Low). By the third hour, upward motions are first predicted at both the north and the south coasts of the lake, while downward motions are apparent over the lake. By the sixth hour, a well-defined positive vertical velocity region (lake-breeze convergence zone) along the upwind and the lateral sides of the lake becomes obvious. Two major vertical velocity maxima are predicted by the model along the convergence zone at both the lateral sides. The vertical velocity cell that forms over the southwest lateral side of the lake is larger compared to the cell that forms northeast of the lake. This is believed to be due to the backing of the wind caused by cold air advection from the lake to the warmer land. By the ninth and twelfth hours, this area of large vertical motion along the southwest lateral side of the lake moves inland, while the other cell northeast of the lake remains essentially stationary. The lake-breeze convergence zone is also advected northwestward in the general direction of the mean flow by the southeasterly ambient wind. In the late afternoon, magnitudes of the vertical velocities increase. For example, the maximum upward motion reaches a magnitude of about 17 cm s^{-1} by twelfth hour for the southwestern cell, while the corresponding magnitude of the vertical velocity for the northeastern cell is about 9 cm s^{-1}.

These regions of strong vertical motions would therefore be preferred locations for maximum convergence and consequently convective precipitation. In contrast, intensities of the upward motions along the upwind side of the lake are relatively weaker as compared to those along both the lateral sides. This must be due to the fact that when southeasterly ambient flow advects the convergence zone over relatively smoother and cooler lake surface, cooling effect of the lake-breeze suppresses upward motions in this region as compared to those over the land along the lateral sides of the lake. Since the lake has a symmetric circular shape, one would except symmetric lake-breeze convergence zone around the lake. However, an asymmetric lake-breeze convergence zone forms in the late afternoon. This is believed to be due to the combined effect of the Coriolis force and the differential surface roughness between the land and the water.

As shown in Fig. 4, a well-defined subsidence region is also predicted by the model over the lake during the integration. This is of course due to horizontally divergent nature of the lake-breeze circulation. The subsidence region occurs over the lake ahead of the lake-breeze convergence zone in the general direction of the ambient flow. In the latter stages this downward motion region is advected northwestward along with the lake-

breeze convergence zone by the ambient wind. Existence of the subsidence region would lead to a cloud free region over the lake.

Cross sections after 3 and 12 hours of simulation at Grid #25 in the y-direction provides additional information about the movement and the development of updrafts and downdrafts as well as the thermal structure of the atmosphere (Fig. 5). As can be seen in the figure, weak downdrafts over the lake and weak updrafts at both the lateral sides of the lake begin to develop early in the morning. The surface temperature discontinuities at the land-water interface (Grid #18 and 34) caused by the continuous differential heating between the land and the water during the day is a major factor in the formation of the updrafts and downdrafts. Once the convective low-level structure forms, the associated updrafts penetrate increasingly upward. In the late afternoon, the updrafts are advected to Grids 6–7 and 28–30, while the downdrafts stay almost stationary over the lake. The magnitude of both the updrafts and the downdrafts increase significantly between 3–12 hours of simulation.

The associated thermodynamic structure of the cross sections provides further information about the characteristics of the mesoscale circulations induced by a circular lake on a synoptically undisturbed day. The cross section of potential temperatures shows that a symmetric thermal structure begins to develop near the land-water interfaces at low-levels by the third hour. In the later stage, a highly convective PBL is fully developed by the twelfth hour. The height of the PBL can be clearly identified from the simulated sounding of the potential temperature (Fig. 6). Figure 6 shows simulated profiles of the potential temperature after 12 hours of simulation at Grids #10 and 25 of Fig. 5. Solid line shows the vertical profile over the lake and dashed line the vertical profile over the land. The temperature profile over the lake indicates a transition layer between the underlying layer of lower stability and the stable layer of the free atmosphere, while the vertical profile of potential temperature over the land shows a well-developed convective mixed layer. The potential temperature remains more or less uniform in the mixed layer. This layer is dominated by buoyancy generated turbulance, except during evening transition hours when shear effects become important. Just before sunset (12 hours of simu-

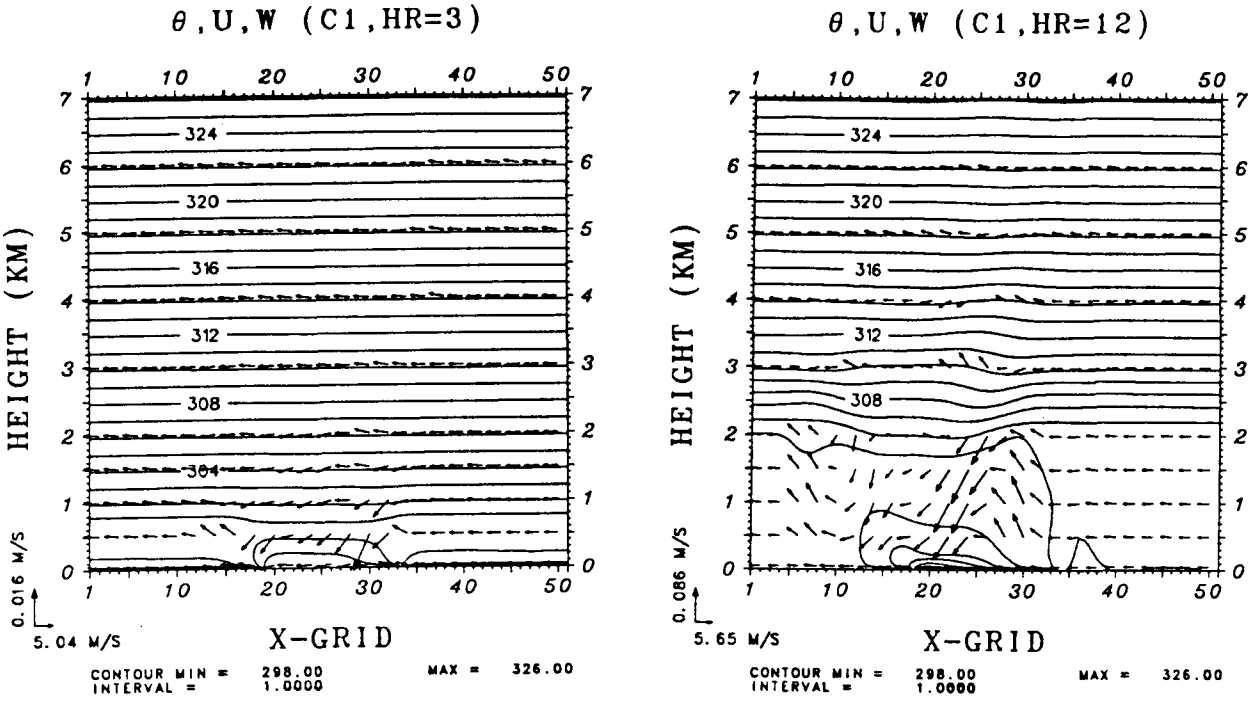

Fig. 5. Cross section of potential temperature (θ) and east-west and vertical components (u and w) after 3 and 12 hours of simulation for the southeasterly wind Case C1 at Grid #25 in the y-direction ($J = 25$). The maximum u and w are plotted at the left corner of the figure

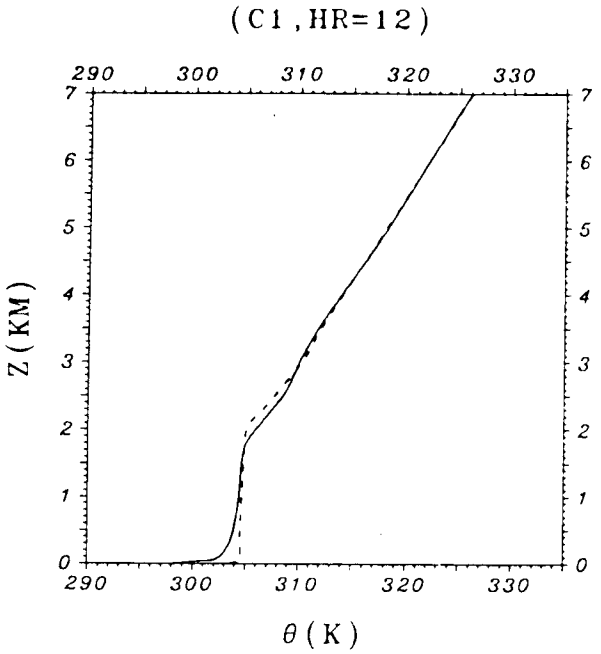

Fig. 6. Simulated potential temperature profiles (θ) at Grid #10 and #25 of Fig. 5 after 12 hour of simulation for the southeasterly wind Case C1. Solid line shows the vertical profile over lake, while dashed line shows the profile over land

lation), there is a net radiative loss of energy from the surface and, consequently, an inversion begins to form at the surface. The surface heating over land during the day leads to an upward exchange of sensible heat and subsequent warming of the lowest layer due to heat flux convergence. This process progressively causes development of a convective boundary layer over the land whose depth grows higher with time as compared to the boundary layer height over the lake (Fig. 6).

Distributions of the predicted cloud water (q_c) at the height of their largest values after 3, 6, 9 and 12 hours of simulation for the southeasterly wind case are presented in Fig. 7. The results show that the formation of the convective clouds is highly correlated with the development of the lake-breeze convergence zone (Fig. 4), as one would expect. In the early morning (third hour of model integration), the clouds do not form, because upward motions are not strong enough at this time. During the afternoon as the low-level convergence increases, the clouds begin to form along the upwind and the lateral sides of the lake and increase in depth in conjunction with the lake-breeze convergence. For example, the predicted cloud water reaches its largest magnitude of about $7\,g\,kg^{-1}$ at 1500 m after 6 hours of simulation, while it reaches a value of about $54\,g\,kg^{-1}$ at 2000 m after 12 hours of simulation indicating significant growth of the clouds by late afternoon. The convective clouds develop only along the lake-breeze convergence zone, while a persistent cloudless region is always present over the lake during the integration. Cloudless region over lakes is well documented by other investigators (e.g. Frank et al., 1967; Pielke, 1974).

Two major deep convective cloud regions are predicted by the model along the lateral sides of the lake associated with intense convergence in these regions, while deeper and stronger clouds develop only over the southwest lateral side of the lake associated with stronger vertical motions. Thus convective precipitation would develop only along the lateral sides of the lake. By the twelfth hour, very little precipitation (about 0.01 mm) occurs over the southwest lateral side of the lake (not shown). However, significant precipitation develops in the late afternoon after the development of substantial lake-breeze induced convergence. For example, predicted cumulative rain water (q_r) at the surface associated with the precipitating clouds after 14 hours of simulation is shown in Fig. 8. Relatively larger precipitation (about 7 mm) occurs over the southwest lateral side of the lake associated with strong convection over this area, while very little precipitation (0.001 mm) develops northeast of the lake.

The results presented above indicate that the lake-breeze circulation is essentially a horizontally divergent phenomena over the lake but has a strong influence on the formation of both the convergence zone and consequent convection around the lake. Strong upward motions and associated convection develop along the lateral sides of the lake for the southeasterly mean flow. Also largest convection occurs over land southwest of the lake for this mean wind direction in response to the backing of the winds caused by cold air advection over a warmer surface.

3.2 Case C2. Southwesterly Wind

A southwesterly flow of about $6.0\,m\,s^{-1}$ ($U_g = 4.2\,m\,s^{-1}$ and $V_g = 4.2\,m\,s^{-1}$) was used to study the influence of another ambient wind direction on the lake-breeze circulations and associated

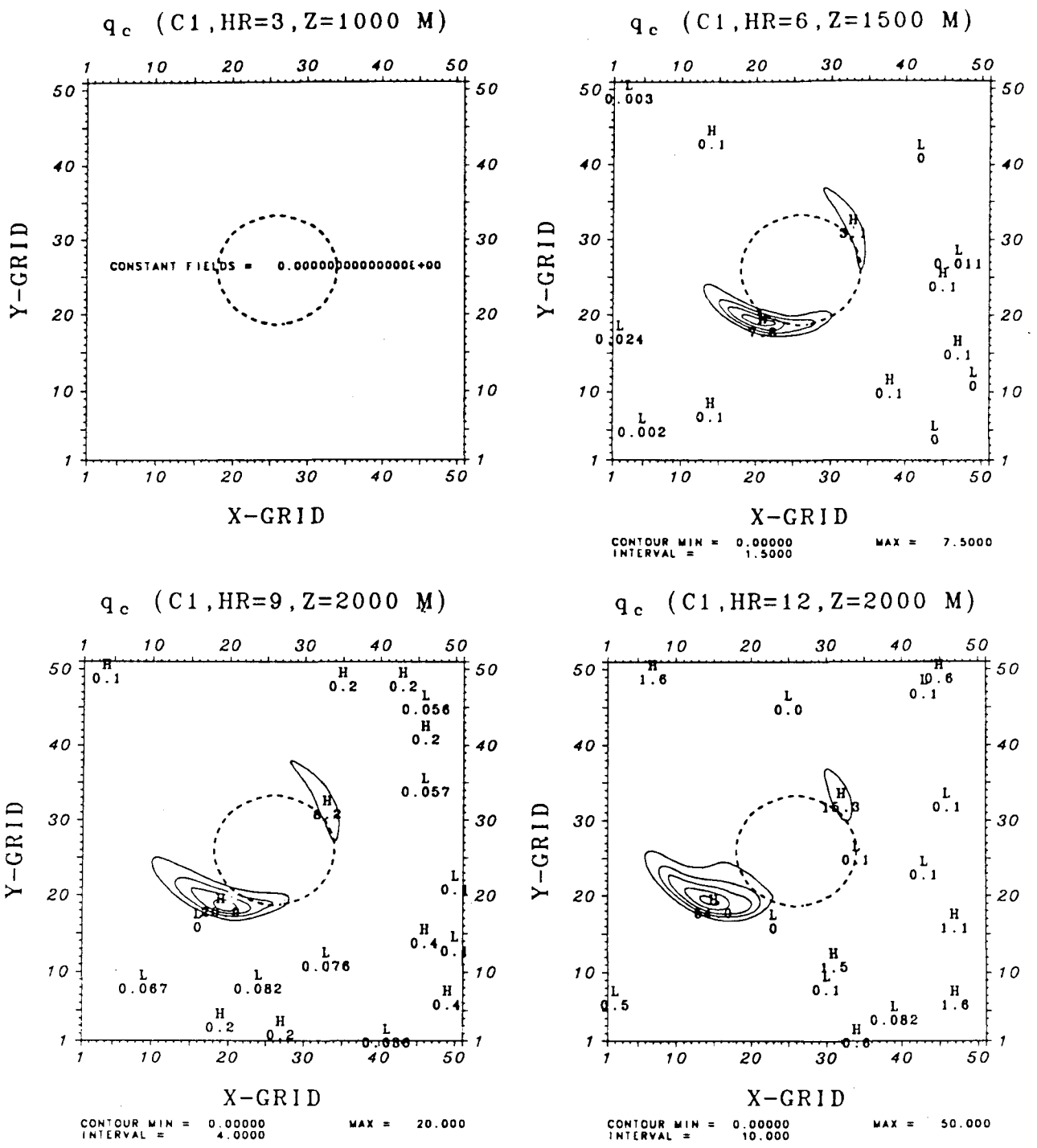

Fig. 7. The cloud water q_c (g kg^{-1}) at the heights where they had their largest values after 3, 6, 9 and 12 hours of simulation for the southeasterly wind Case C1. The extremes are indicated by letters *H* (High) and *L* (Low)

convection in this case study. All prescribed model parameters are the same as those in Case C1 except wind direction. The ambient wind direction is now different by 90°. Under southwesterly ambient wind, the predicted variables (u, v, w, q_c and q_r) appear to have a pattern similar to those found in the earlier case study under southeasterly ambient wind. This is to be expected due to the symmetric shape of the circular lake. The differences that occur between the two cases must exclusively be

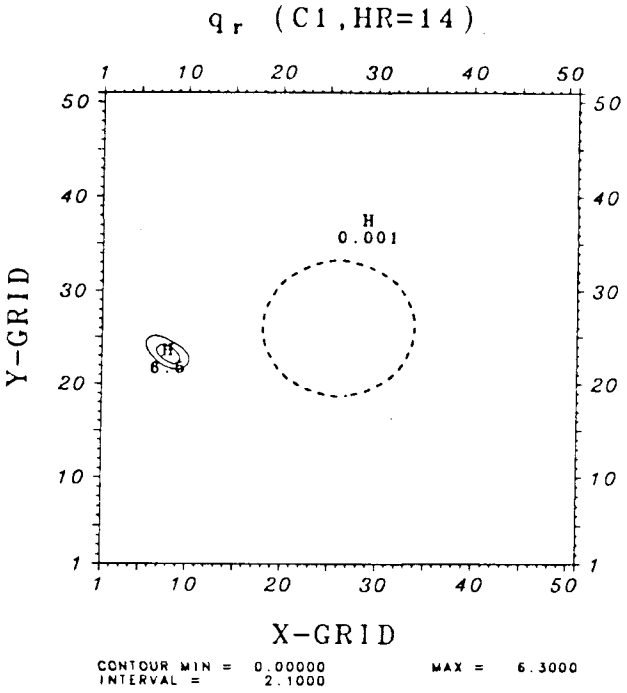

Fig. 8. The rain water q_r (mm/total hour) at the surface after 14 hours of simulation for the southeasterly wind Case C1. The extreme is indicated by letter *H* (High)

caused by the orientation of the wind with respect to the lake. Therefore, only the vertical velocity and precipitation distributions will be presented here for brevity.

The predicted vertical velocities for the southwesterly ambient wind are given in Fig. 9. In contrast to Case C1, early in the morning by the third hour, upward motions are predicted only along east and west coasts of the lake. By the sixth hour, the lake-breeze convergence zone forms along the lateral and the upwind sides of the lake oriented in the general direction of the mean flow. Two vertical velocity maxima form along both the lateral sides (northwest and southeast) of the lake, while largest vertical motion occurs northwest of the lake. Later in the afternoon, by the ninth and twelfth hours of simulation, this largest cell moves inland, while the other cell southeast of the lake remains almost stationary. A subsidence region is always present over the lake. The convergence zone and the subsidence region are advected northeastward in the general direction of the ambient flow. Figure 10 shows predicted cumulative rain water associated with the upward motions presented in Fig. 9 at the surface after 14 hours of simulation for the southwesterly ambient wind. Meager precipitation (about 0.01 mm) occurs by the twelfth hour (not shown) only at a location northwest of the lake. Relatively larger precipitation develops only after the intensification of the lake-breeze convergence zone by the fourteenth hour at the same location, while little precipitation is produced east of the lake associated with the second largest upward motion area in Fig. 9.

A comparison of the results from Case C2 with those in Case C1 emphasizes the importance of the influence of ambient wind direction on the lake-breeze convergence patterns and hence convection. Magnitudes of the predicted variables are generally the same in both the cases due to the symmetric shape of the lake. Differences between the two case studies generally occur mainly due to the orientation of the lake with respect to the wind direction. Spatial and temporal variations of the predicted lake-breeze convergence zone and hence the convection are found to be basically controlled by the ambient wind direction. For both the wind directions the lake-breeze convergence zone and the convection develop along the upwind and the lateral sides of the lake with respect to the direction of the ambient flow. However, for a noncircular lake, changes in wind direction could cause differences not only in the magnitude of the predicted variables but also in the location of the predicted variables between the two cases. Coastal irregularities generally cause local regions of enhanced low-level convergence and consequent large upward motions (e.g., McPherson, 1970; Boybeyi and Raman, 1992).

3.3 *Case C3. Influence of Lake Size*

This case study is designed to determine the effect of lake size on lake-breeze patterns and associated convection. For Case C3, a southwesterly ambient wind is prescribed, but with a reduced lake size. All model parameters are the same as those in Case C2 except the lake size. The radius of the lake is reduced from 60 to 44 km.

Since the patterns of predicted variables are essentially the same as in Case C2, only the predicted vertical velocities are presentd here for Case C3 (Fig. 11). Although the patterns are the same, significant differences occur in the magnitude of the vertical velocities between the two case studies. For example, by the twelfth hour, largest value of vertical velocity is predicted to be about

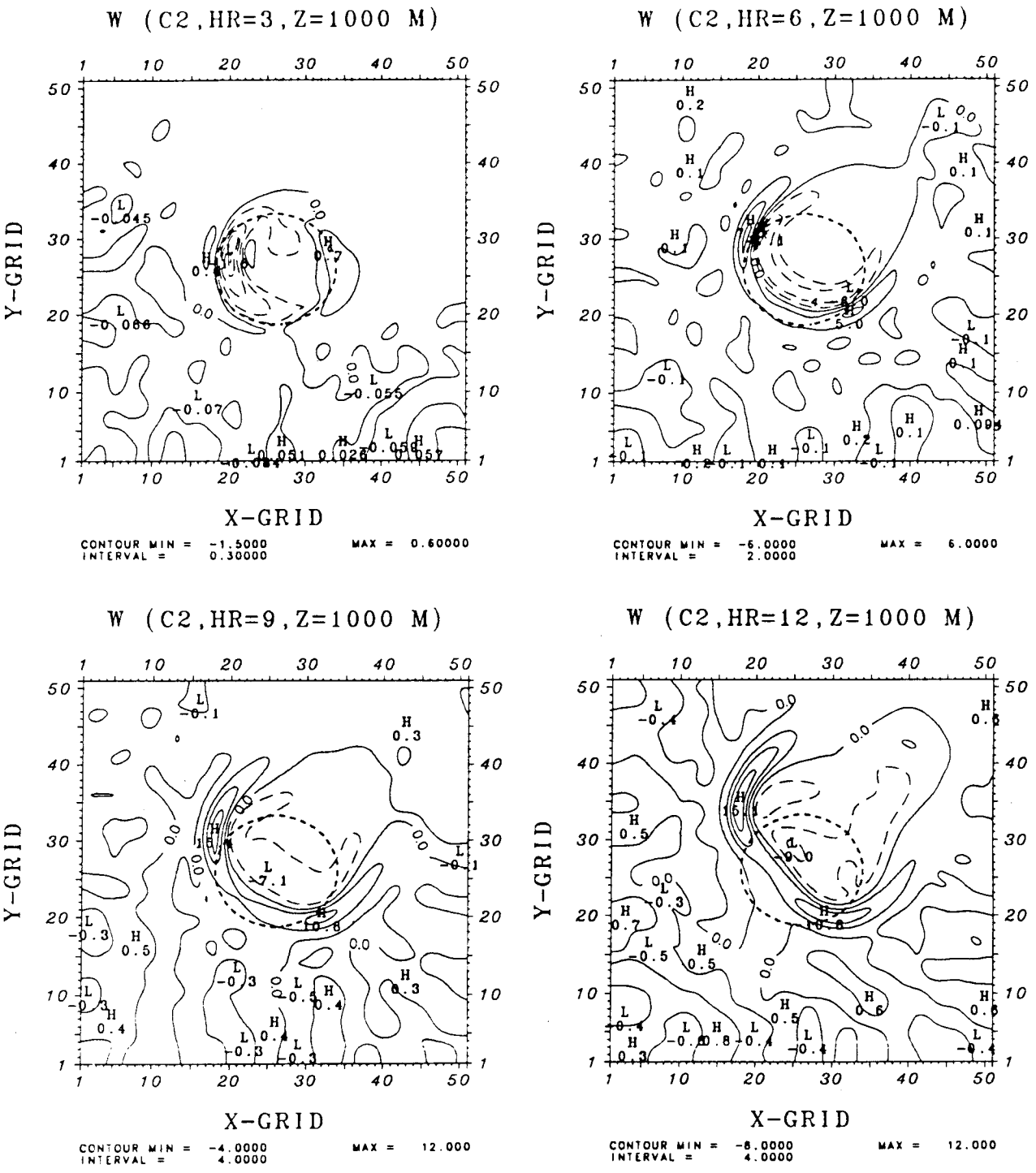

Fig. 9. The vertical velocity W (cm s^{-1}) at 1000 m after 3, 6, 9 and 12 hours of simulation for the southwesterly wind Case C2. The extremes are indicated by letters H (High) and L (Low)

7 cm s^{-1} in Case C3, while it had a value of about 15 cm s^{-1} in Case C2 at the equivalent time. The difference is believed to be due to the reduced lake size. Two similar studies were conducted by Neumann and Mahrer (1974, 1975) on circular lakes and circular islands. Neumann and Mahrer (1975) found that the lake-breeze front of a large lake is much better developed than that of a small lake. However, they concluded, based on their previous study on a circular island (Neumann

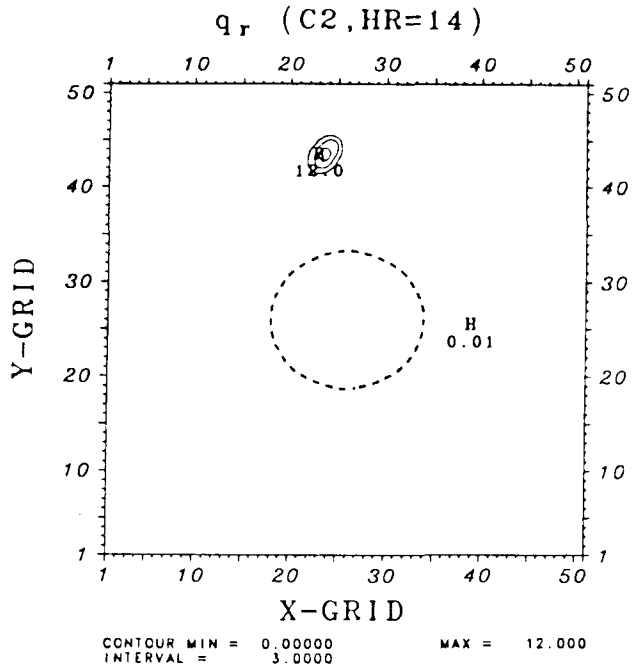

Fig. 10. The rain water q_r (mm/total hour) at the surface after 14 hours of simulation for the southwesterly wind Case C2. The extreme is indicated by letter *H* (High)

and Mahrer, 1974), that the differences in magnitudes between the two lake sizes is a nonlinear function and hence, cannot be linearly extrapolated by the difference in size. Nonlinearity is due to the fact that the smaller lake is more divergent than the larger lake because of its small size. In a similar manner, strong horizontal divergence of the lake-breeze of a small lake Case C3 prevents the lake-breeze convergence zone from growing as fully as that found in Case C2 for large lake case. Consequently, the vertical velocities are smaller in Case C3 than those in Case C2. Also convections are not as strong as those predicted in Case C2 for the large lake case (not shown). For example, in this case study precipitation does not occur during the integration in contrast to the Case C2, because the magnitude of the vertical motions are smaller. This indicates that the lake size plays an important role in determining the strength of lake-breeze convergence zones and associated convection.

3.4 Case C4. Calm Wind

Sensitivity of the convection to the wind speed is investigated in this case study using a nearly calm southwesterly ambient wind. All the model parameters are the same as those in Case C2 except that calm winds are assumed ($U_g = 0.1\ \mathrm{m\,s^{-1}}$ and $V_g = 0.1\ \mathrm{m\,s^{-1}}$).

The predicted horizontal winds (U and V) at 50 m, vertical velocity (W) at 1000 m, cloud water (q_c) at the height where it had its largest value and rainwater (q_r) at the surface after 10 hours of simulation for this case are shown in Fig. 12. The results are presented only at the tenth hour of simulation. In contrast to the southeasterly and southwesterly ambient winds, all the predicted variables are almost equally prevalent around the entire coast of the lake and they remain almost stationary during the day. Figure 12a shows that under calm wind conditions the lake-breeze is a well-defined horizontally divergent phenomena resulting in a well-defined lake-breeze convergence zone around the entire coastline of the lake. The winds propagate inland in a direction normal to the coasts and increase in speed. Note that the wind speed is larger along the coastlines than anywhere else. During the integration, the convergence zone remains almost stationary and shows little movement during the day (not shown). Thus it appears that the distance that the lake breeze convergence zones and the associated variables penetrate inland is also a function of the magnitude of the ambient wind. In other words, the lake breeze convergence zone appears to move inland at a fraction of the ambient wind speed. The predicted vertical motions (Fig. 12b) are almost parallel to the coast. The predicted cloud pattern associated with the convergence zone also shows similar behavior aligning parallel to the coast (Fig. 12c). Deep convective clouds develop to the northwest of the lake associated with the intense upward motions producing precipitation close to the coastline (Fig. 12d) over this region. Later in the afternoon (12 hours of integration), precipitation occurs all around the coastline of the lake (not shown).

A comparison of the results for the predicted variables (w, q_c, and q_r) in Fig. 12 with those for both Case C1 and Case 2 shows that the magnitudes of the predicted variables in Case C4 after 10 hours of simulation are larger than those found in Case C1 and Case C2 even after 12 hours of simulation. For example, 1.5 mm precipitation is produced in Case C4 after 10 hours of simulation, while precipitation is not produced in Case C1 and Case C2 by this hour. A precipitation of 0.01 mm occurs in Case C1 and Case C2 only after 12 hours of simulation. This is due to the fact that stronger

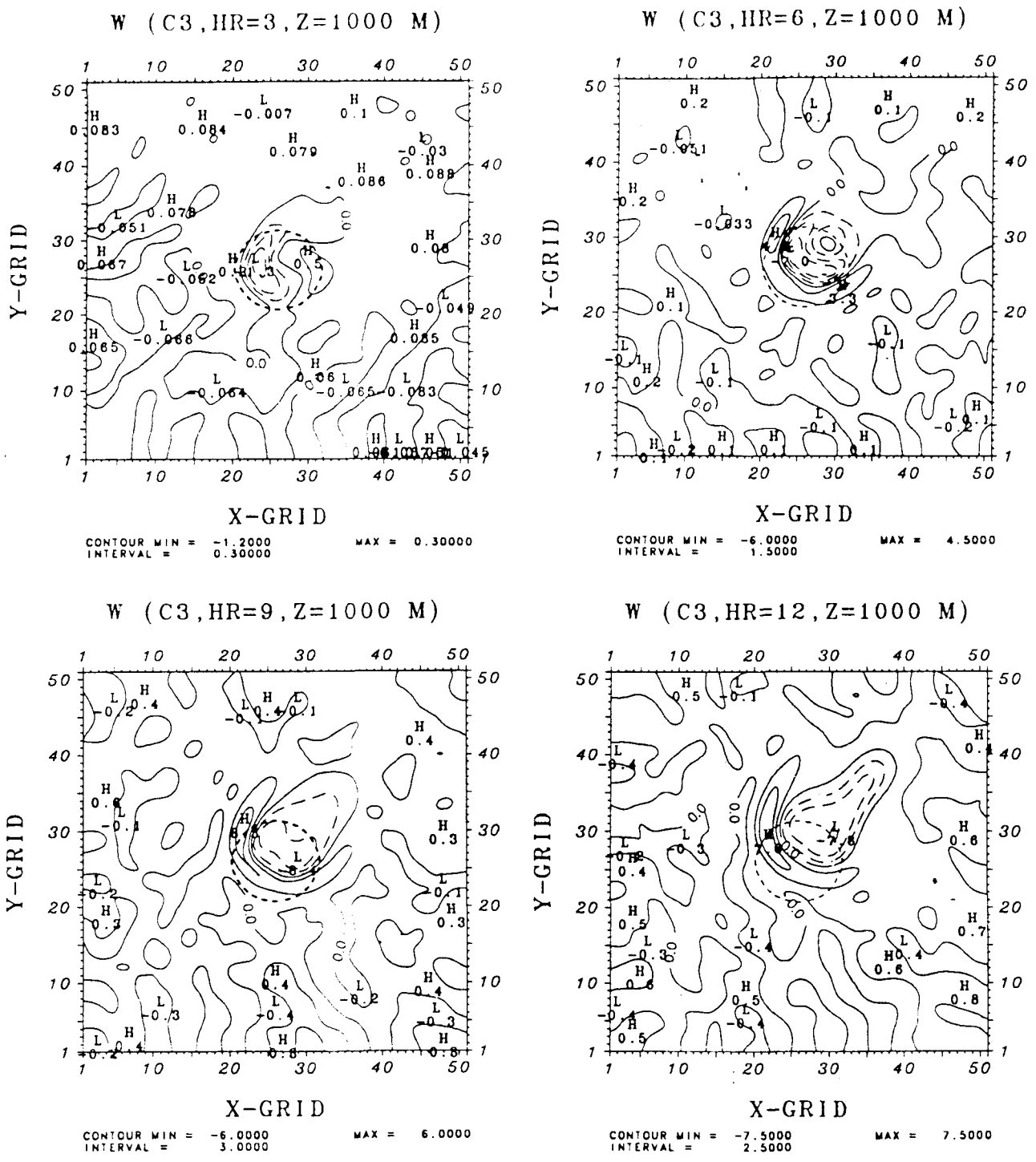

Fig. 11. The vertical velocity W (cm s^{-1}) at 1000 m after 3, 6, 9 and 12 hours of simulation for the southwesterly wind Case C3, but the lake size is reduced. The extremes are indicated by letters H (High) and L (Low)

ambient winds in Case C1 and Case C2 produce a less vigorous lake-breeze as observations indicate (Frank et al., 1967). One of the reasons could be that the convergence zone is advected faster with stronger ambient wind conditions. However, the convergence zone remains nearly stationary under calm ambient wind condition and thus has more time to develop in its original environment. These results indicate that the magnitude of the ambient wind is also an important factor in the formation

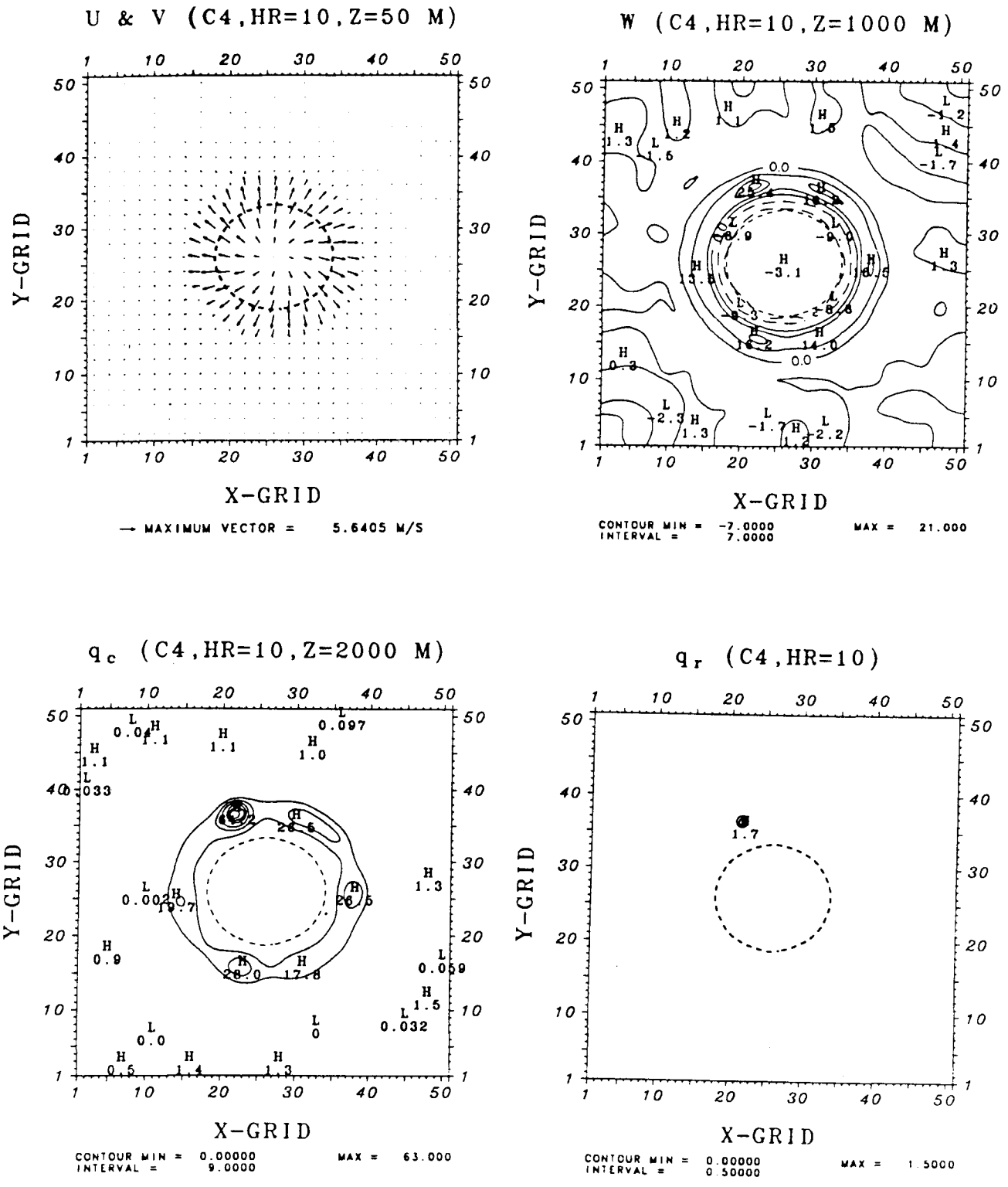

Fig. 12. The low-level horizontal winds U and V ($m\,s^{-1}$) at 50 m, vertical velocity W ($cm\,s^{-1}$) at 1000 m, cloud water q_c ($g\,kg^{-1}$) at the height where it had its largest value and rain water q_r (mm/total hour) at the surface after 10 hours of simulation for the calm southwesterly wind Case C4

of lake-breeze convergence zone and associated convection.

3.5 *Case C5. Influence of Surface Roughness*

The relative importance of differential surface roughness on mesoscale circulations over the lake is examined in this case study. The intent here is to ignore spatial variation of the surface roughness. Therefore, values of all the prescribed model parameters are set identical to those in Case C2 (southwesterly ambient wind case) except that the surface roughness lengths over land and water are assumed initially to be equal to 0.0015 cm.

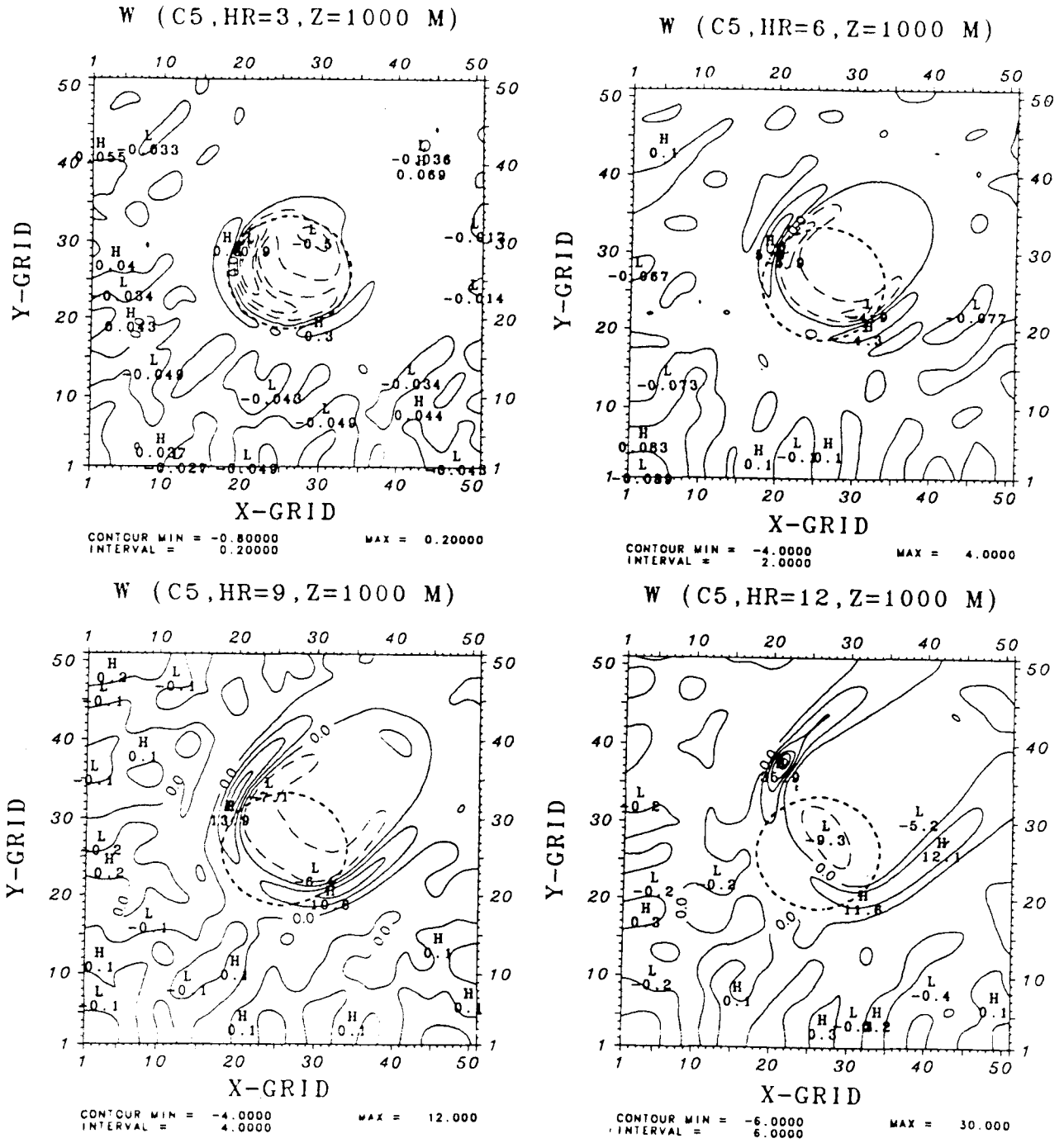

Fig. 13. The vertical velocity W (cm s^{-1}) at 1000 m after 3, 6, 9 and 12 hours of simulation for the southwesterly wind Case C5, but no differential surface roughness. The extremes are indicated by letters *H* (High) and *L* (Low)

Then, their values are calculated over the water by using the Charnock's relationship given by

$$z_0 = 0.018 \frac{u_*^2}{g}$$

where surface roughness length (z_0) is determined by friction velocity (u_*) and gravitational acceleration (g). The basic assumptions implied in Charnock's relationship are that the winds are blowing steadily and long enough for the wave field to be in equilibrium with the wind field and that the surface is aerodynamically rough. The surface roughness over water surface is thus related to both the wind and the wave fields. Although this relation is inappropriate over land, same values of z_0 determined by Charnock's relationship over water at each time step are assumed to be valid over land. Thus the spatial variation of the surface roughness between the land and the water is ignored. Hence this case study will investigate the influence of differential surface roughness between the land and water on mesoscale lake-breeze circulations. Note that surface roughness values were assumed to be constant as 4 cm over land, while Charnock's relationship was used over the water in Case C2 so that there was significant spatial variation of the surface roughness.

The predicted vertical velocities for Case C5 are given in Fig. 13. A comparison of the results between Case C2 and Case C5 shows large differences in the magnitudes of vertical motions between the two cases, although the predicted patterns are the same. The magnitudes in Case C5 are predicted to be smaller than those in Case C2 at least until the end of the ninth hour of simulation (Fig. 13). For example, the magnitude of the vertical velocity reaches a value of about 13 cm s^{-1} at the ninth hour of the simulation in Case C5, while it has a value of about 15 cm s^{-1} at the equivalent time in Case C2. This must be due to the larger surface roughness values over land in Case C2. As one would anticipate, the larger surface roughness values increase the vertical turbulent transfer of heat from the ground early in the day in Case C2 as the surface heating increases. The vertical convective mixing carries a larger amount of heat upward with the result that the air over the rougher land is warmer. This leads to the increase in land-lake temperature difference causing pressure to fall more rapidly over the land. Therefore, the vertical velocities in Case C2 at least for the first nine hours of simulation are larger than those in Case C5 in response to the rapid pressure fall. However, the predicted vertical velocity values in Case C5 become larger than those in Case C2 later in the afternoon. For example, the magnitude of the vertical velocity reaches a value of about 35 cm s^{-1} at the twelfth hour of the simulation in Case C5, while it has a value of 15 cm s^{-1} at the equivalent time in Case C2. This is probably due to the fact that the larger surface roughness values increase the vertical transfer of momentum in the afternoon as the surface heating decreases resulting in more rapidly slowed down low-level horizontal winds by the surface friction in Case C2 as compared to Case C5. This causes less intense low-level convergence and hence generates smaller vertical velocities in Case C2 as compared to Case C5 later in the day. Therefore, the surface friction plays an important role in determining the distance that the lake-breeze convergence zone is advected by the ambient flow. For example, the convergence zone is advected further northeastward in Case C5 than in Case C2 due to smaller surface roughness values in Case C5 (Figs. 9d and 13d).

A comparison of the results of both the case studies also shows that differential surface roughness between the land and the lake seems to play an important role in the formation of the asymmetric shape of the convergence zone. For example, by the twelfth hour of the simulation, the lake-breeze convergence zone in Case C5 (Fig. 13d) is more symmetrical than that found in Case C2 (Fig. 9d). The other important factor for the formation of an asymmetric shape of the convergence zone could be the Coriolis force and its effect will be investigated in the next section.

3.6 Case C6. Influence of the Coriolis Force

The results presented in the previous case studies have suggested that the predicted asymmetrically-shaped lake-breeze convergence zone around the circular lake may be also due to the Coriolis force. Therefore, it was decided to investigate the influence of the Coriolis force on the formation of the lake-breeze convergence zone in this case study by ignoring the effect of the Coriolis force. All the other prescribed model parameters were the same as those in Case C1.

The predicted vertical velocities for Case C6 are presented in Fig. 14. A comparison of the results

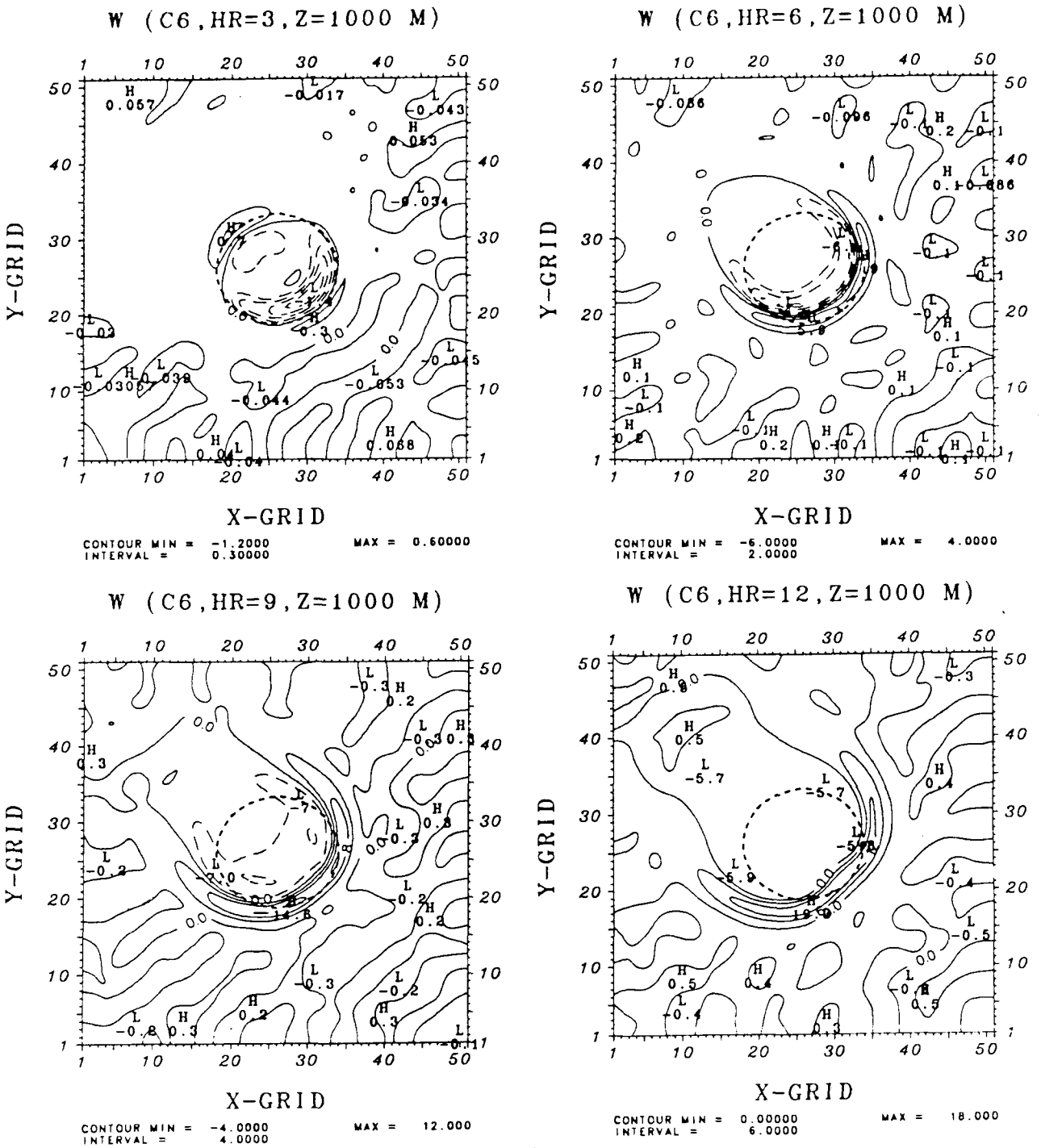

Fig. 14. The vertical velocity W (cm s^{-1}) at 1000 m after 3, 6, 9 and 12 hours of simulation for the southeasterly wind Case C6, but no Coriolis force. The extremes are indicated by letters H (High) and L (Low)

between Case C1 and Case C6 shows significant differences in the patterns of the lake-breeze convergence zone. For example, by the ninth and twelfth hours of the simulation, a symmetric lake-breeze convergence zone in Case C6 (Fig. 14) forms around the lake compared to the one in Case C1 (Fig. 4). This clearly shows that the presence of the Coriolis force is one of the responsible mechanisms in producing asymmetric lake-breeze convergence zone around the circular lake. The other major

difference occurs in the magnitudes of the predicted vertical velocities. For example, in Case C1 two maximum vertical velocity cells are predicted at both the lateral sides of the lake with the largest one located southwest of the lake (Fig. 4). Also the magnitude of these cells are larger than that predicted along the upwind side of the lake in Case C1. However, in Case C6 in the absence of the Coriolis force, the magnitude of the predicted vertical velocities are distributed almost uniformly along the lake-breeze convergence zone. In the absence of the Coriolis force, the pressure gradient force is balanced only by friction force so that the friction force becomes larger in Case C6 as compared to Case C1. Therefore, the convergence zone is advected less in Case C6 toward the northwest which is the general direction of the mean flow for the southeasterly ambient wind.

3.7 *Case C7. Influence of Baroclinic Ambient Wind*

The influence of baroclinic ambient wind condition on lake-breeze patterns is examined in this case study. All prescribed model parameters are the same as those in Case C1 except that geostrophic vertical wind shear is used to initialize the model. The values of the geostrophic wind and the geostrophic vertical wind shear are assumed as follows;

$$U_g = -4.2\,\mathrm{m\,s^{-1}}, \frac{\delta U_g}{\delta z} = \begin{cases} 2\,\mathrm{ms^{-1}\,km^{-1}}, & Z \leqslant 5\,\mathrm{km} \\ 0, & Z > 5\,\mathrm{km} \end{cases}$$

$$V_g = 4.2\,\mathrm{m\,s^{-1}}, \frac{\delta V_g}{\delta z} = \begin{cases} -1\,\mathrm{ms^{-1}\,km^{-1}}, & Z \leqslant 5\,\mathrm{km} \\ 0, & Z > 5\,\mathrm{km} \end{cases}$$

which corresponds to a southeasterly geostrophic wind of about $6\,\mathrm{m\,s^{-1}}$ at the surface with both speed and directional geostrophic wind shear up to 5 km. The geostrophic wind shear is assumed zero above the 5 km height.

The predicted vertical velocities for this case study are shown in Fig. 15. A comparison of the results from Case C7 with those in Case C1 for barotropic initial conditions (Fig. 4) emphasizes the importance of the influence of baroclinity on the lake-breeze convergence patterns. By the sixth hour, a lake-breeze convergence zone forms along the lateral and the upwind sides of the lake oriented in the general direction of the mean flow with two vertical maxima along both the lateral sides (northwest and southeast) of the lake. The pattern of the convergence zone by this time is similar to that found in Case C1 (Fig. 4). However, when the baroclinity becomes sufficiently large in the afternoon the pattern of the lake-breeze convergence zone differs from in Case C1. By the ninth and twelfth hours, the lake-breeze convergence zone along the northeast lateral side of the lake shifts almost to south of the lake, while the lake-breeze convergence zone along the southwest lateral side of the lake moves toward the north due to the directional geostrophic wind shear component. Note that at the equivalent time (12 hours of simulation) as in Case C1, the lake-breeze convergence zone along the northeast lateral side of the lake remains essentially stationary, while the convergence zone along the southwest lateral side of the lake moves toward the southwest of the lake. Also the advection of the lake-breeze convergence zone is slower in Case C7 than in Case C1 due to the geostrophic shear component. For example, by the twelfth hour, the convergence zone moves further in the general direction of the mean flow in Case C1 as compared to Case C7. This is due to the fact that the magnitude of the ambient wind is weaker in Case C7 due to the assumed geostrophic speed shear component.

Another major difference between the two cases occurs in the magnitude of the predicted vertical velocities. Magnitudes of the vertical velocities are larger in Case C7 than those in Case C1 at all equivalent times. This is believed to be due to vertical wind shear which produces more turbulence and hence stronger vertical eddy fluxes of heat within the boundary layer.

Cross sections of potential temperature and east-west and vertical wind components provide more information about development of updrafts (Fig. 16). A comparison of cross sections of baroclinic (Fig. 16) to nonbaroclinic (Fig. 5) simulations shows significant differences between the two cases. The vertical variation of velocity divergence resulting from the vertical wind shear is important in modifying the vertical atmospheric structure. The magnitudes of both the updrafts and the downdrafts are stronger in Case C7. Consequently the PBL height over land is slightly larger than that found in Case C1, while the PBL height over water is slightly lower. By the third hour, southeasterly ambient flow changes its direction at upper levels resulting in an asymmetric thermal structure in low-levels as compared to that found in Case C1

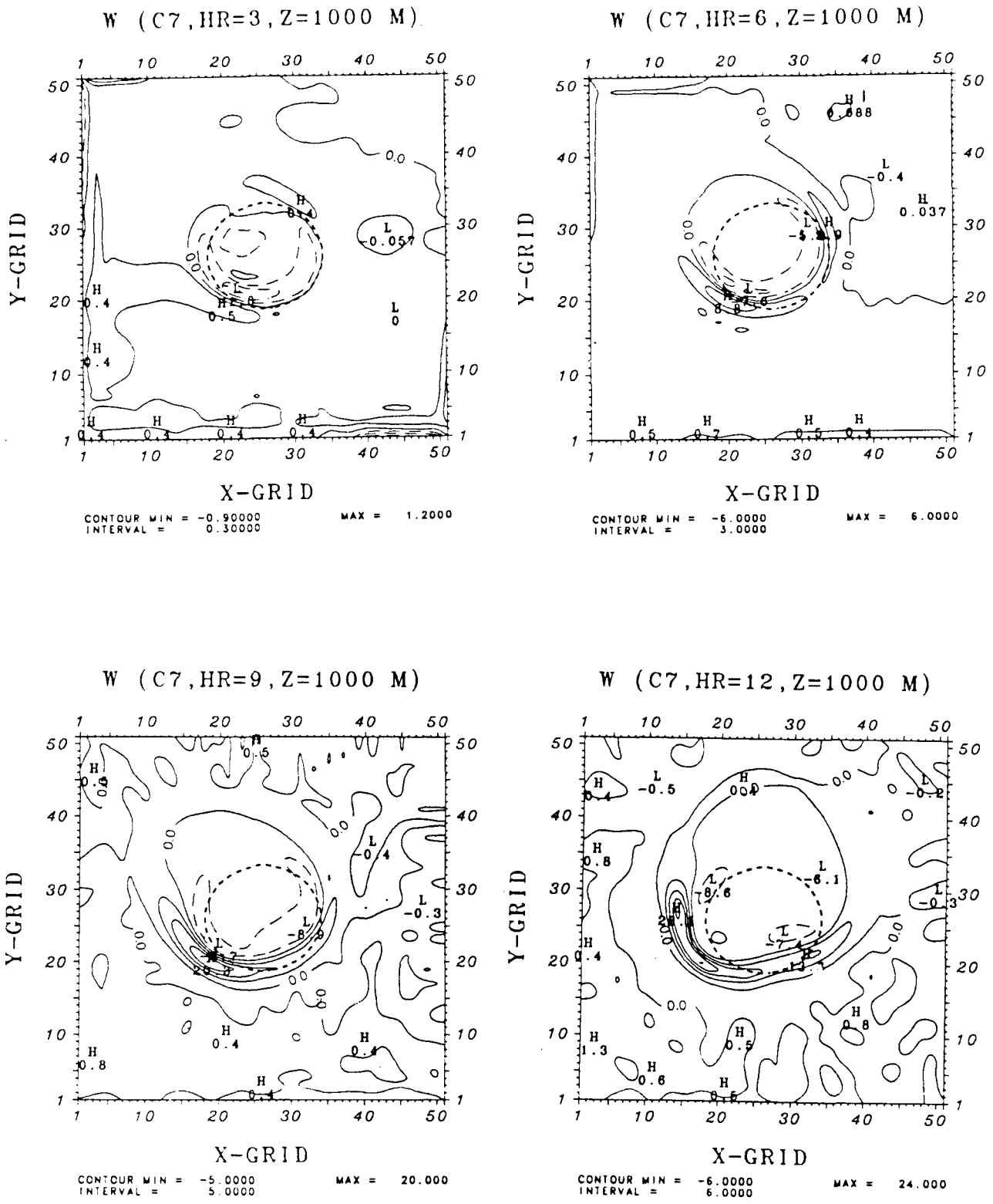

Fig. 15. The vertical velocity W (cm s^{-1}) at 1000 m after 3, 6, 9 and 12 hours of simulation for the southeasterly wind with geostrophic vertical wind shear Case C7. The extremes are indicated by letters H (High) and L (Low)

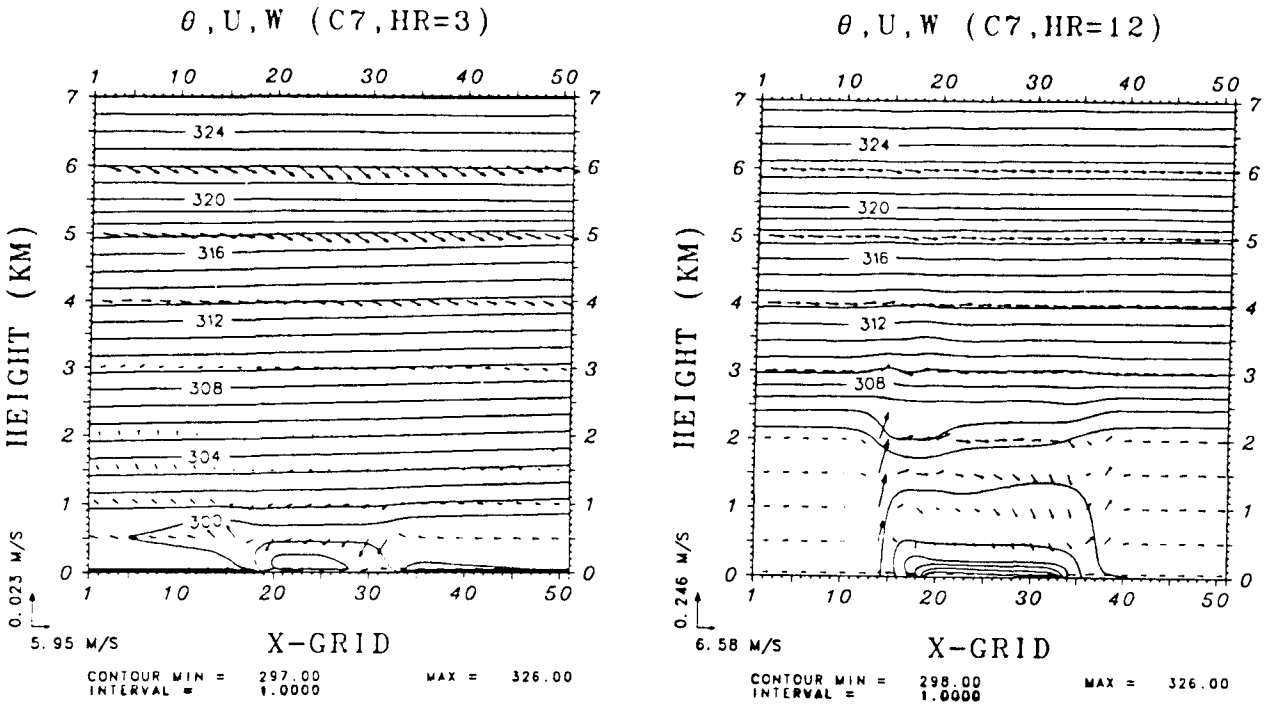

Fig. 16. Cross section of potential temperature (θ) and east-west and vertical components (u and w) after 3 and 12 hours of simulation for the Case C7 at Grid #25 in the y-direction ($J = 25$). The maximum u and w are plotted at the left corner of the figure

(Fig. 5). By the twelfth hour, the low-level winds also change their directions. This leads a more symmetric thermal structure. These results indicate that the baroclinity of the atmosphere has a profound influence in mesoscale atmospheric circulations.

4. Conclusions

The relationship between mesoscale lake-breeze circulation and convection is investigated over a circular lake for typical undisturbed summer days by using a higher order turbulence closure mesoscale boundary layer model under different environmental control mechanisms. The numerical sensitivity experiments conducted in this study included the influence of lake-land temperature difference, two different ambient wind directions, the ambient wind speed, lake size, surface roughness, the Coriolis force, and vertical wind shear on the formation of the lake-breeze convergence zone and associated convection.

It was concluded that the lake-breezes are essentially divergent phenomena over the lake. The divergent flow of the lake-breezes causes a well defined lake-breeze convergence zone around the lake. The spatial and the temporal variations of this lake-breeze convergence zone and hence, convection are generally controlled by the characteristics of the ambient flow. Under southeasterly and southwesterly ambient winds, the lake-breeze convergence zone forms along the lateral and upwind sides of the lake with respect to the general direction of the ambient wind. Intense convection occurs for both the southeasterly and the southwesterly winds along the lateral sides of the lake in conjunction with the convergence zone in the late afternoon. Somewhat weaker convective clouds and no precipitation occur over the upwind side of the lake. This indicates that an important factor controlling the development and evolution of convection over a circular lake is the formation of the lake-breeze. In contrast to the southeasterly and southwesterly wind cases, under a calm ambient wind condition the predicted features are prevalent almost equally around the coastline of the lake and show little movement during the day. Southeasterly ambient winds produced almost the same intense convection as compared to southwesterly ambient winds because of the symmetric shape of the lake. The maximum values under both the wind directions were

generally smaller than those predicted under calm ambient winds due to the fact that stronger ambient winds produce less vigorous lake-breezes.

Experiments conducted to examine the effect of lake size have shown that the lake size has an important effect in intensifying convection. Since the small lake is more divergent than the large lake, the strong horizontal divergence of the breeze associated with a smaller lake prevents the formation of a well defined convergence zone. This prevents the convection from growing as fully as those found for larger lakes. Also a persistent cloudless region over the lake during the day is predicted in all cases. Surface roughness values over land appears to influence the location and the magnitude of the convection by determining the intensity of the vertical transfer of heat and momentum. It is found that the combined effect of the differential surface roughness and the Coriolis force is the responsible mechanism for producing asymmetric lake-breeze convergence zone around a circular lake. Finally, it is also found that the initial baroclinic flow modifies mesoscale lake-breeze circulation patterns. When the baroclinity becomes sufficiently large in the afternoon the pattern of the lake-breeze convergence zone and the magnitude of the predicted variables considerably differ from those predicted under barotropic initial conditions.

Our future research will address mesoscale diffusion processes coupling a Lagrangian particle model with the mesoscale PBL model.

Acknowledgements

This work was supported by the U.S. Army Research Office under Contract DAAL03-91-G-0214.

References

Boybeyi, Z., Raman, S., 1992: A three-dimensional numerical sensitivity study of convection over the Florida peninsula. *Bound.-Layer Meteor.* (in press).

Briggs, W. G., Graves, M. E., 1962: A lake breeze index. *J. Appl. Meteor.*, **1**, 474–480.

Businger, J. A., Wyngaard, J. C., Izumi, Y., Bradley, E. F., 1971: Flux-profile relationships in the atmospheric surface layer. *J. Atmos. Sci.*, **28**, 181–189.

Estoque, M. A., 1981: Further studies of a lake breeze. Part I: Observational study. *Mon. Wea. Rev.*, **109**, 611–618.

Estoque, M. A., Gross, J. M., 1981: Further studies of a lake breeze. Part II: Theoretical study. *Mon. Wea. Rev.*, **109**, 619–634.

Frank, N. L., Moore, P. L., Fisher, G. E., 1967: Summer shower distribution over the Florida peninsula as deduced from digitized radar data. *J. Appl. Meteor.*, **6**, 309–316.

Hjelmfelt, M. R., 1990: Numerical study of the influence of environmental conditions on lake-effect snowstorms over lake Michigan. *Mon. Wea. Rev.*, **118**, 138–150.

Hjelmfelt, M. R., Braham, R. R., Jr., 1983: Numerical simulation of the airflow over Lake Michigan for a major lake-effect snow event. *Mon. Wea. Rev.*, **111**, 205–219.

Huang, C. Y., 1990: A mesoscale planetary boundary layer model for simulations of topographically induced circulations. Ph.D. dissertation, North Carolina State University, 253 pp.

Huang, C. Y., Raman, S., 1991: Numerical simulation of January 28 cold air outbreak during GALE. Part I: The model and sensitivity tests of turbulence closures. *Bound.-Layer Meteor.*, **55**, 381–407.

Huang, C. Y., Raman, S., 1988: A numerical modeling study of the marine boundary layer over the gulf stream during cold air advection. *Bound.-Layer Meteor.*, **45**, 251–290.

Klemp, J. B., Durran, D. R., 1983: An upper boundary condition permitting internal gravity wave radiation in a mesoscale numerical model. *Mon. Wea. Rev.*, **111**, 430–444.

Lavoie, R. L., 1972: A mesoscale numerical model of lake-effect storms. *J. Atmos, Sci.*, **29**, 1025–1040.

Mahrer, Y., Pielke, R. A., 1977: The effects of topography on the sea and land breeze in a two-dimensional model. *Mon. Wea. Rev.*, **105**, 1151–1162.

McPherson, R. D., 1970: A numerical study of the effect of a coastal irregularity on sea breeze. *J. Appl. Meteor.*, **9**, 767–777.

Mellor, G. L., Yamada, T., 1982: Development of a turbulence closure model for geophysical fluid problems. *Rev. Geophys. Space Phys.*, **20**, 851–875.

Miller, M. J., Thorpe, A. J., 1981: Radiation conditions for the lateral boundaries of limited area numerical models. *Quart. J. Roy. Meteor. Soc.*, **107**, 615–628.

Neumann, J., Mahrer, Y., 1974: A theoretical study of the sea and land breezes of circular islands. *J. Atmos. Sci.*, **31**, 2027–2039.

Neumann, J., Mahrer, Y., 1975: A theoretical study of the lake and land breezes of circular lakes. *J. Atmos. Sci.*, **103**, 474–485.

Orlanski, I., 1976: A simple boundary condition for unbounded hyperbolic flows. *J. Comput. Phys.*, **21**, 251–269.

Pearson, R. A., 1973: Properties of the sea breeze front as shown by a numerical model. *J. Atmos. Sci.*, **30**, 1050–1060.

Pielke, R. A., 1974: A three-dimensional numerical model of the sea breeze over south Florida. *Mon. Wea. Rev.*, **102**, 115–139.

Walsh, J. E., 1974: Sea breeze theory and applications. *J. Atmos. Sci.*, **31**, 2012–2026.

Warming, R. F., Kutler, P., Lomax, H., 1973: Second- and third-order noncentered difference schemes for nonlinear hyperbolic equations. *AIAA.*, **11**, 189–196.

Authors' address: Z. Boybeyi and S. Raman, Department of Marine, Earth and Atmospheric Sciences, North Carolina State University, Raleigh, NC 27695-8208, U.S.A.